JOURNAL OF COMPUTATIONAL PHYSICS 118, 356–365 (1995)

An Eulerian Vlasov–Hilbert Code for the Numerical Simulation of the Interaction of High-Frequency Electromagnetic Waves with Plasma

A. GHIZZO, T. RÉVEILLÉ, AND P. BERTRAND

L.P.M.I., Université de Nancy-I, 54506 Vandoeuvre les Nancy cedex, France

T. W. JOHNSTON

I.N.R.S. Energie et Matériaux (Université du Québec), Varennes, J3X 1S2 Canada

J. LEBAS

L.P.M.I., Université de Nancy-I, 54506 Vandoeuvre les Nancy cedex, France

AND

M. SHOUCRI

Centre Canadien de Fusion Magnétique, Varennes, J3X 1S1 Canada

Received May 2, 1994; revised October 17, 1994

In order to handle one-dimensional spatial problems in plasmas with very high frequency electromagnetic waves ($\omega \gg \omega_p$), the 1 – 1/2D Eulerian Vlasov code has been modified to interface with the ponderomotive force associated with the complex envelopes of the high frequency electromagnetic fields rather than the fields themselves. The ponderomotive force for the Vlasov code has been computed from the complex amplitude equations and the real Vlasov density perturbations have been converted to complex amplitude form for the mode equations via the Hilbert transform. The resulting Vlasov–Hilbert code allows us to handle high-frequency problems with complex amplitude equations for high frequency electromagnetic waves with the Vlasov code only for the relatively low-frequency plasma wave. Computations are made with this model to situations typical of *forward Raman scattering* and *beatwave*; results are in accordance with other computational methods such as full electromagnetic Vlasov–Maxwell code or envelope equations whenever they can be used. This model provides a saving of order $(\omega_{pump}/\omega_{plasma})^2$ (i.e., time × space) in computer time, as compared with the direct full electromagnetic Vlasov–Maxwell method with the highest space-time resolution required.

I. INTRODUCTION

In recent years considerable plasma simulation [1–5] has been done using what we have termed an Euler–Vlasov code allowing unequalled precision in the examination of details of the electron distribution function in action phase space (with one longitudinal degree of freedom) for various plasma problems. An important application of interest is the beatwave driven acceleration of electrons, for which the experimental ratios of driver frequency to plasma frequency are very high ($\omega_0/\omega_p = 37$ in Ref. [6] and $\omega_0/\omega_p = 100$ in Ref. [7]). These high ratios impose a prohibitive computer burden on a direct attack via Euler–Vlasov or particle-in-cell (PIC) simulation. (The burden is doubly severe because an exact approach requires spatial resolution of very small wavelengths, together with the small time step required for the high driver frequency).

In this paper we discuss the implementation of a hybrid solution to this problem. The full Vlasov apparatus is used for the longitudinal plasma wave aspect of the problem, but with the addition of the ponderomotive force driver, which is itself obtained from complex amplitude (i.e., complex envelope) coupled wave equations for the electromagnetic driver waves (and any other important electromagnetic sidebands). The time step is thus only a fraction of a plasma period and the spatial resolution is a fraction of the light plasma wavelength. Given complex electromagnetic wave envelopes, the calculation of the real ponderomotive force required by the Vlasov electrostatic code obviously presents no difficulty. The innovation here (at least for plasma simulation applications) is in the calculation of the complex amplitude envelope of the plasma wave which is required at each time step for coupling with the driver waves and which must reflect just those plasma aspects (such as nonlinear detuning and energy transfer of energy to the electrons) which are the reason for interest in the problem in the first place. For

0021-9991/95 $6.00

the generation of the complex envelope of the plasma wave we use the spatial Hilbert transform. For this reason we refer to this hybrid system as a Vlasov–Hilbert (or VH) code.

In passing we note that the technique can of course be applied to a PIC system. Although the (usually significant) PIC noise may cause some problems, the potential of PIC codes in two or more dimensions would seem to make such an effort worthwhile.

Until now this Hilbert transform has been used in some of our previous Euler–Vlasov code results [5] as a simple diagnostic to aid comparison with theory. While Vlasov or PIC codes can of course furnish full space-time detail (usually in space snapshots) for fields, currents, and densities, this is often in a form that has too much detail to improve understanding (an example of the phenomenon characterized as "trying to drink from a firehose"). The common coin of theory is in fact the complex amplitude as used in mode-coupling theory. A very useful bridge between simulation and theory is thus provided by the time evolution of the complex space envelopes calculated from spatial Hilbert transforms. It was the success of these comparisons, together with the noiseless character of the Euler–Vlasov code, that led us to the Vlasov–Hilbert method.

In this paper we present three examples of the use of the Vlasov–Hilbert code, together with two types of comparison, on the one hand with the full Vlasov code (where the frequency ratios permit) and on the other with the conventional coupled-mode results.

The presentation of this work is as follows. In Section II the Vlasov–Hilbert code is discussed, as well as some comparisons between the model and a full electromagnetic Vlasov code, together with a simple nonlinear three-wave envelope model (which includes linear loss and approximative relativistic detuning). The simplest case of a periodic system is considered in detail in Section III, including the check of the conservation of the Manley–Rowe invariants. Then, in Section IV, the model is applied to a system which is not spatially periodic, with externally incident beatwave drivers at modest value for the pump wave frequencies (close to $\omega_0 = 2.60\omega_p$ and $\omega_1 = 1.53\omega_p$), allowing close comparison between the Vlasov–Hilbert model, the Maxwell–Vlasov model and the canonical three-wave model. Section V contains an example of high-frequency beatwave ($\omega_{0,1} \approx 30\omega_p$) using the Hilbert–Vlasov code and comparison with the coupled-mode model. Finally in Section VI, we present the major conclusions.

II. THE RELATIVISTIC VLASOV–HILBERT CODE

(A) *The Full Electromagnetic Vlasov–Maxwell Code*

First, let us recall briefly the main features of one-dimensional electromagnetic Vlasov–Maxwell code. In order to handle the plasma velocities relevant to future particle accelerators, the model equation must at least be relativistic in the acceleration direction (x). For the linear (y-direction) laser polarisation intensities we consider here the transverse dynamics can be economically included in the nonrelativistic transverse cold fluid approximation. The Vlasov equation in the acceleration (x) direction is thus

$$\frac{\partial f}{\partial t} + \frac{p_x}{m\gamma}\frac{\partial f}{\partial x} e\{E_x + u_y B_z\}\frac{\partial f}{\partial p_x} = 0, \tag{1}$$

where $\gamma = \sqrt{1 + p_x^2/m^2c^2}$. Defining $P_z(x, t) = mu_y$ as the nonrelativistic fluid transverse momentum, we have in the y direction:

$$\frac{\partial P_y}{\partial t} = -eE_y. \tag{2}$$

The electrostatic longitudinal self-consistent field E_x obeys the Poisson's equation with ions forming a fixed neutralizing background n_0,

$$\frac{\partial^2 \varphi}{\partial x^2} = \frac{e}{\varepsilon_0}(n_e(x, t) - n_i), \tag{3}$$

where $n_e(x, t)$ is the electron density defined by

$$n_e(x, t) = \int_{-\infty}^{+\infty} f(x, p_x, t)\, dp_x. \tag{4}$$

The transverse electromagnetic field of course obeys Maxwell's equations:

$$\frac{\partial B_z}{\partial t} = -\frac{\partial E_y}{\partial x}, \tag{5}$$

$$\frac{\partial E_y}{\partial t} = -c^2\frac{\partial B_z}{\partial x} - \frac{J_y}{\varepsilon_0}, \tag{6}$$

where $J_y = -en_e(x, t)u_y(x, t)$.

Defining $E^{\pm} = E_y \pm cB_z$, Eqs. (5) and (6) can be rewritten in a more suitable form

$$\left(\frac{\partial}{\partial t} \pm c\frac{\partial}{\partial x}\right)E^{\pm} = -\frac{J_y}{\varepsilon_0} \tag{7}$$

which enables the solution of Maxwell's equations along their vacuum characteristics $x \pm ct = \text{const}$ (see [8]). Hence we have to prescribe the boundary conditions on $E^+(t)$ at $x = 0$ and $E^-(t)$ at $x = L$, where L denotes the length of the system. In the present simulations, we have considered

$$\begin{aligned} E^+(x = 0, t) &= \sqrt{2}E_0 \sin \omega_0 t + \sqrt{2}E_0 \sin \omega_1 t \\ E^-(x = L, t) &= 0, \end{aligned} \tag{8}$$

corresponding to a radiation field entering the plasma at $x = 0$ and exiting at $x = L$.

(B) *The Vlasov–Hilbert Code*

To handle the problem of high frequency electromagnetic waves (for which full detail would require calculations over very short intervals in time and space), we replace the Maxwell's equations for transverse waves by a three-wave model coupled to the Vlasov equation. Only envelope equations for the pump and idler (Stokes) are considered here. Assuming the vector potential A_y of the electromagnetic wave in the form

$$A_y(x, t) = \tfrac{1}{2}A_0(x, t)e^{i(k_0x-\omega_0t)} + \tfrac{1}{2}A_1(x, t)e^{i(k_1x-\omega_1t)} + \text{c.c.}, \quad (9)$$

where 0 and 1 refer, respectively, to the electromagnetic pump components of the wave vector, the envelope equations for A_0 and A_1 can be written with $\omega_0 = \omega_1 + \omega_e$ and $k_0 = k_1 + k_e$ (ω_e, k_e being respectively the frequency and wave number of the electron plasma wave) as

$$\left(\frac{\partial}{\partial t} + v_{g_0}\frac{\partial}{\partial x}\right)A_0 = -\frac{i\omega_p^2}{4\omega_0 n_0}A_1\rho_e \quad (10a)$$

$$\left(\frac{\partial}{\partial t} + v_{g_1}\frac{\partial}{\partial x}\right)A_1 = -\frac{i\omega_p^2}{4\omega_1 n_0}A_0\rho_e^*, \quad (10b)$$

where

$$n_0, \rho = \tfrac{1}{2}\rho_e(x, t)e^{i(k_ex-\omega_et)} + \text{c.c.} \quad (11)$$

denote the unperturbed homogeneous electron density and the perturbed density, respectively. ρ_e is given by the Hilbert transform of the density perturbations from the Vlasov code. The group velocities are the standard values for electromagnetic waves in plasma (with $i = 0, 1$, we have $v_{g_i} = (1 - \omega_p^2/\omega_i^2)^{1/2}c$).

The Vlasov equation used in the Hilbert–Vlasov model is

$$\frac{\partial f}{\partial t} + \frac{p_x}{m\gamma}\frac{\partial f}{\partial x} + \{-eE_x + F(x, t)\}\frac{\partial f}{\partial p_x} = 0, \quad (12)$$

where $F(x, t) = (e^2/2m)(\partial(A^2)/\partial x)$ is the ponderomotive force.

Both Vlasov and envelope equations are integrated using a time-splitting scheme of the usual kind. The different steps used for integrating the Vlasov and envelope equation are indicated in Fig. 1.

A three successive shifts sequence is used to evolve the electron distribution function f and slowly varying complex amplitude for $A_{0,1}$ from $t_n = n\Delta t$ to $t_{n+1} = (n + 1)\Delta t$:

Step 1. Between t_n and t_{n+1}, shift in the x direction for a time $\Delta t/2$,

$$f(x, p_x, t_{n+1/2}^-) = f\left(x - \frac{p_x}{m\gamma}\frac{\Delta t}{2}, p_x, t_n\right), \quad (13a)$$

together with

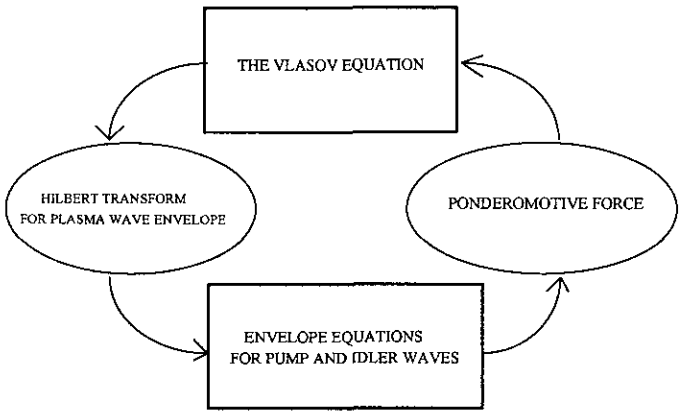

FIG. 1. Global scheme of the Vlasov–Hilbert code: The scheme summarizes the interesting possibility of handling high-frequency beatwave problems with complex amplitude equation for pump, idler (Stokes), and using the Vlasov equation for the relatively low-frequency plasma wave.

$$A_{0,1}(x, t_{n+1/2}^-) = A_{0,1}(x - v_{g_{0,1}}\Delta t/2, t_n). \quad (13b)$$

Step 2. Compute the longitudinal field E_x at time $t_{n+1/2}$ using Poisson's equation and then the real perturbed density $g(x, t) = (n_e(x, t) - n_0)/n_0$. The integration of the envelope equation involves knowledge of the complex amplitude of plasma mode ρ_e at time $t_{n+1/2}$. The complex envelope curve for the rapidly oscillating phases is obtained by using a spatial Hilbert transform of the mode, effected as follows: The signal g if Fourier transformed, and the positive k modes are multiplied by $+i$, while the negative k modes are multiplied by $-i$. The resulting function is Fourier transformed back g_{Hilbert}, which results in a Hilbert transform. Then the complex amplitude ρ_e is given by the relation $\rho_e(x, t) = a(x, t)e^{i\psi(x,t)}$ with $a(x, t) = \sqrt{g^2 + g_{\text{Hilbert}}^2}$ and the phase $\psi(x, t)$ obeys $\tan\psi = g_{\text{Hilbert}}/g$. We compute the envelope equation at time $t_{n+1/2}$ as follows:

$$A_0(x, t_{n+1/2}^+) = A_0(x, t_{n+1/2}^-) - \frac{i\omega_p^2\Delta t}{4\omega_0 n_0}A_1(x, t_{n+1/2}^-)\rho_e(x, t_{n+1/2}^-) \quad (14a)$$

$$A_1(x, t_{n+1/2}^+) = A_1(x, t_{n+1/2}^-) - \frac{i\omega_p^2\Delta t}{4\omega_1 n_0}A_0(x, t_{n+1/2}^-)\rho_e^*(x, t_{n+1/2}^-). \quad (14b)$$

The real ponderomotive force for the electron Vlasov equation is then calculated using the relation

$$F(x, t) = \frac{e^2}{2m}\frac{\partial(A^2)}{\partial x} = \frac{e^2}{4m}[ik_eA_0A_1^* \exp i(k_ex - \omega_et) + \text{c.c.}] \quad (15)$$

which allows us to compute the electron distribution function at time $t^+_{n+1/2}$ (by a shift in the p_x space for a time Δt) and we obtain

$$f(x, p_x, t^+_{n+1/2}) = f[x, p_x - (-eE_x^{n+1/2} + F(x, t^-_{n+1/2}))\Delta t, t^-_{n+1/2}]. \tag{16}$$

Step 3. Between $t^+_{n+1/2}$ and t_{n+1} we shift again in the x direction for a time $\Delta t/2$:

$$f(x, p_x, t_{n+1}) = f\left(x - \frac{p_x}{m\gamma}\frac{\Delta t}{2}, p_x, t^+_{n+1/2}\right) \tag{17a}$$

$$A_{0,1}(x, t_{n+1}) = A_{0,1}(x - v_{g_{0,1}}\Delta t/2, t^+_{n+1/2}). \tag{17b}$$

The boundary conditions for the electromagnetic amplitude are then given by

$$A_0(x = 0, L) = \frac{E_0\xi_{\text{profile}}(t)}{\omega_0\sqrt{2}} \tag{18a}$$

$$A_0(x = L, t) = 0 \tag{18b}$$

$$A_0(x = 0, L) = \frac{E_0\xi_{\text{profile}}(t)}{\omega_0\sqrt{2}} \tag{18c}$$

$$A_1(x = L, t) = 0, \tag{18d}$$

where the initial increase in time τ of the electromagnetic waves to a constant value is modeled by the function ξ_{profile} given by

$$\xi_{\text{profile}}(t) = \begin{cases} \sin^2(\pi t/2\tau) & \text{if } t \le \tau \\ 1 & \text{if } t \ge \tau \end{cases} \tag{19}$$

The simulation is done as long as the launched electromagnetic waves do not reach the other boundary; this explains relations (18b) and (18d).

(C) *The Three-Wave Model*

Because we wish eventually to make comparisons between results given by (i) the full electromagnetic Vlasov–Maxwell model, (ii) an envelope three-wave model, and (iii) those obtained by a Vlasov–Hilbert code and to discuss action conservation, we found it convenient to develop also a three-wave code. Together with Eqs. (10a) and (10b), which describe the evolution of electromagnetic modes, the plasma mode must be also taken into account. We recall for reference that in the fluid model, the plasma mode is generated by the resonant coupling between both pumps and is described by [4]

$$\left(\frac{\partial}{\partial t} + v_{g_e}\frac{\partial}{\partial x} + \gamma - i\delta_{\text{rel}}|\rho_e|^2\right)\rho_e = -\frac{ie^2k_e^2n_0}{4m^2\omega_e}A_0A_1^*, \tag{20}$$

where the relativistic correction has been retained in the plasma wave envelope equation through the term $\delta_{\text{rel}} = 3\omega_e^3/8k_e^2c^2n_0^2$ and v_{g_e} denotes the electron fluid plasma wave group velocity $v_{g_e} = 3k_ev_{\text{th}}^2/\omega_e$, v_{th} being the electron thermal velocity. Equations (10a), (10b), and (20) are also integrated by using a splitting scheme.

III. SIMULATION RESULTS AND THE MANLEY–ROWE ACTION RELATIONS

In a recent publication using periodic geometry treated in Ref. [4], we have applied the Manley–Rowe action relations to the problem of SRS in the forward direction, as simulated by the Eulerian Maxwell–Vlasov code in periodic geometry. The action sum of the pump and the scattered SRS wave was well conserved, while the action loss between the pump and plasma wave was shown to be well accounted for in detail by examining the electron energy for electrons above the lower trapping boundary (separatrix) in the $x - p_x$ phase space. Thus the utility was clearly demonstrated for using action conservation to separate the effects of three-wave interaction from those due to nonlinear particle–wave interaction. These simulation results on action evolution are now compared with the solution given by the Vlasov–Hilbert code in the case of the SRS instability. First recalling the necessary definitions from the previous Euler–Vlasov code work [4].

In the three-wave parametric decay from the pump wave "0" to the scattered wave "s" and the lossy electron plasma wave "e," we have, as usual,

$$k_0 = k_s + k_e, \quad \omega_0(k_0) + \Delta\omega = \omega_s(k_s) + \omega_e(k_e). \tag{21}$$

(We assumed perfect k-matching—since we have a periodic simulation and match mode numbers exactly—while $\Delta\omega/\omega_p \ll 1$ contains the mismatch). The complex action density amplitudes were defined as

$$a_0 = \left(\frac{\varepsilon_0\omega_0}{2}\right)^{1/2}A_0, \quad a_s = \left(\frac{\varepsilon_0\omega_s}{2}\right)^{1/2}A_s \tag{22a}$$

$$a_e = i\left(\frac{\omega_e}{2\varepsilon_0}\right)^{1/2}\frac{\rho_e}{k_e\omega_p}. \tag{22b}$$

With this definition, the action density S ($=aa^*$) is then given from the energy density W (in SI units) by (see [4])

$$s = aa^* = \frac{W}{\omega} = \frac{\langle\text{Energy density}\rangle_\omega}{\omega} = \frac{1}{4\omega}\left[\mu_0H^2 + \varepsilon_0E\left(\frac{\partial\omega\varepsilon_r}{\partial\omega}\right)E^*\right]. \tag{23}$$

The envelope equations (10a) and (10b) for A_0, A_s become then for a_0, a_s (as previously mentioned in Ref. [4])

$$\left(\frac{\partial}{\partial t} + v_{g_0}\frac{\partial}{\partial x}\right) a_0 = -\Gamma a_s a_e e^{i\Delta\omega t} \tag{24a}$$

$$\left(\frac{\partial}{\partial t} + v_{g_s}\frac{\partial}{\partial x}\right) a_s = \Gamma a_0 a_e^* e^{-i\Delta\omega t} \tag{24b}$$

with

$$\Gamma = \frac{e}{2m}\frac{k_e\omega_p}{(2\varepsilon_0\omega_0\omega_s\omega_e)^{1/2}}. \tag{24c}$$

On dropping the $\partial/\partial x$ envelope terms, as one can here for this uniformly excited spatially periodic case, we obtained the usual action sums, including loss,

$$C_s = S_0 + S_s = |a_0|^2 + |a_s|^2 = \frac{W_0}{\omega_0} + \frac{W_s}{\omega_s} = C_s(t=0) \tag{25a}$$

$$C_e(t) = S_0 + S_e = |a_0|^2 + |a_e|^2 = \frac{W_0}{\omega_0} + \frac{W_e}{\omega_e}$$

$$= C_e(t=0) - \frac{2\gamma}{m}\int_0^t W_e(t')\,dt'. \tag{25b}$$

Since the velocities are normalized to c, and the frequencies to ω_p, while the electromagnetic pump mode wavenumber was chosen as $8\Delta k$ ($\Delta k = 2\pi/L$ being the fundamental mode), the choice of $k_0(= 2k_s, 2k_e)$ in effect determined the length of system L in terms of c/ω_p. For our plasma temperatures (a two-component plasma was used) a good frequency match was obtained by choosing $k_0c/\omega_p = 2.40$ (and so $k_sc/\omega_p = k_ec/\omega_p = 1.20$). The corresponding frequencies are then $\omega_0 = 2.60\omega_p$ and $\omega_s = 1.534\omega_p$ respectively for pump and Stokes mode, while the plasma frequency is $\omega_e = 1.061\omega_p$, giving a frequency mismatch of $\Delta\omega = \omega_0 - \omega_s - \omega_e = -0.02\omega_p$.

The time behavior of the action densities S_0, S_s from Vlasov–Hilbert simulation are shown together with their sum $C_s = S_0 + S_s$ in Fig. 2a. The corresponding figures obtained for the full electromagnetic Vlasov codes, shown in Ref. [4], are not presented here. However, the Vlasov–Hilbert results obtained here are in excellent agreement with those Vlasov–Maxwell results presented in [4]. As expected, the action sum C_s for undamped electromagnetic wave pair is exactly conserved, indicating that the treatment of the pump and idler waves in the VH model is correctly effected, since the invariant C_s is well conserved, in agreement with the results obtained by the full electromagnetic Vlasov simulation.

In Ref. [4] we have shown that the way to isolate the interaction between the plasma wave interaction with the trapped electrons is to consider the action sum of the pump and plasma wave. These quantities are shown in Fig. 2b. As previously observed in the full electromagnetic Vlasov code, the action sum C_e has a more complicated behavior due to the details of electron trapping, even reversing as the

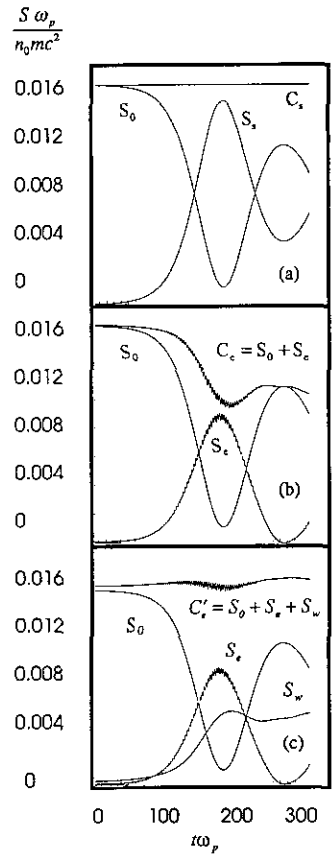

FIG. 2. *The time behavior of the pump (S_0) and idler (S_s) action densities* from the Vlasov–Hilbert simulation, is shown in (a), together with their sum $C_s = S_0 + S_s$, in the case of a periodic system. As expected, the action sum C_s for undamped electromagnetic wave pair is exactly conserved, given good agreement with results obtained in the full electromagnetic simulations. We have plotted in (b) the time behavior of pump (S_0) and plasma wave (S_e) action densities, together with their sum $C_e = S_0 + S_e$, which presents a strong decrease at time $t\omega_p = 200$. The action transfer is taken into account in (c), by considering the "lost action" of particles above the trapping separatrix limit.

plasma wave is decreasing while the pump wave is growing from its minimum value. This interesting feature has been already observed in the full Vlasov code results (thus the treatment of the electric field envelope via the use of the Hilbert transform and of the ponderomotive force in the Vlasov acceleration term do not modify the particle acceleration process). To check this point in detail and by using the trapping separatrix boundary, one can account for the energy in trapped and accelerated electrons. This energy, divided by the plasma oscillation frequency, gives what is defined as the "trapped electron action." Figure 2c shows that the sum of the pump wave action, the plasma wave action and the trapped electron action is nicely conserved. This result makes it clear that the Vlasov–Hilbert model can describe correctly the electron trapping effects and that for this periodic

TABLE I

	Pump wave (0)	Pump wave (1)	Plasma wave
Frequency	$\omega_0 = 2.60\omega_p$	$\omega_1 = 1.534\omega_p$	$\omega_e = 1.065\omega_p$
Wave number	$\frac{k_0 c}{\omega_p} = 2.40$	$\frac{k_1 c}{\omega_p} = 1.164$	$\frac{k_e c}{\omega_p} = 1.236$
Quiver or phase velocity	$\frac{v_{osc_0}}{c} = 0.087$	$\frac{v_{osc_1}}{c} = 0.147$	$v_\varphi = \frac{\omega_e}{k_e} = 0.861c$

case the Vlasov–Maxwell and the Vlasov–Hilbert analyses are in complete agreement.

IV. STUDY OF THE BEATWAVE EXPERIMENT: COMPARISON BETWEEN THE THREE NUMERICAL CODES

We now turn to a more realistic causal test, with an externally incident driver and idler pair with the same frequencies as before.

(A) *Numerical Envelope Calculations*

A series of simulations were performed in the case of a low-frequency beatwave accelerator. Two laser beams with frequencies $\omega_0 = 2.60\omega_p$ and $\omega_1 = 1.562\omega_p$ have been injected in plasma with equal amplitude $E_0/\sqrt{2}$ with $E_0 = 0.320\omega_p mc/e$. The incident electromagnetic wave (ω_0, k_0) and (ω_1, k_1) (corresponding to the pump waves), continuously generated at $x = 0$ drives inside the plasma, a forward-going electron longitudinal plasma wave (ω_e, k_e) according to the matching conditions $\omega_0 = \omega_1 + \omega_e$ and $k_0 = k_1 + k_e$. The simulation parameters are summarized in Table I.

We start with an initial homogeneous Maxwellian plasma (of length $L = 128\lambda_0$, λ_0 being the wave length of the pump wave) and with a thermal velocity $v_{th}/c = 0.17133$ corresponding to a temperature of $T_1 = 15$ keV, with a small fraction (α) of relativistic particles with temperature $T_2 = 100$ keV (see the numerical experiment described in Ref. [4]),

$$f(x, p_x, t = 0) = \frac{(1-\alpha)}{\sqrt{2\pi m T_1}} \exp\left(-\frac{p_x^2}{2mT_1}\right) + \alpha K \exp(-z(\gamma - 1)) \tag{26}$$

with $\alpha = 0.05$, $z = mc^2/T_2$, and $K = (\sqrt{\pi}/4\Gamma(3/2))\,(z\exp(-z)/K_1(z))$ is the normalization constant for a relativistic distribution such that $\int_{-\infty}^{+\infty} f(x, p_x, t = 0)\, dp_x = 1$ (where $K_\nu(z)$ is the usual Bessel function of the third kind). The plasma wave number is $k_e c/\omega_p = 1.236$ which corresponds to $k_e \lambda_D = 0.212$.

The envelopes of the different modes of the rapidly oscillating fields can be obtained in a similar way as in the simulations reported in Ref. [5]. At a given time, the signal is Fourier analysed and thereafter a Hilbert transform is performed, which yields the envelopes of the fields. Figure 3a shows the Hilbert envelopes of the pump wave and idler wave (in action units), computed in the Vlasov–Maxwell code at time $t\omega_p = 200$ while Fig. 3b shows the results obtained by the Vlasov–Hilbert code, at the same time, using the same initial condition.

The corresponding results given by the coupled mode equations (10), (11), and (20) are represented in Fig. 3c in which we have taken a damping term $\gamma = 0$. It is clear that the general features are well reproduced. The major part of the structure in the idler wave is seen to be due to the pump depletion.

Figure 4a and Fig. 4b illustrate respectively the spatial variation of the longitudinal electric field obtained by the Vlasov–Maxwell code and the Vlasov–Hilbert version; together their envelopes are given in action units at the same time. The maximum amplitudes of the waves from both kinetic simulations are roughly the same. There are, however, some distinct differences in shape, indicating dephasing in time. One can see a distinct trend for the Vlasov–Hilbert model to produce somewhat more localized and intense peaks in electrostatic field

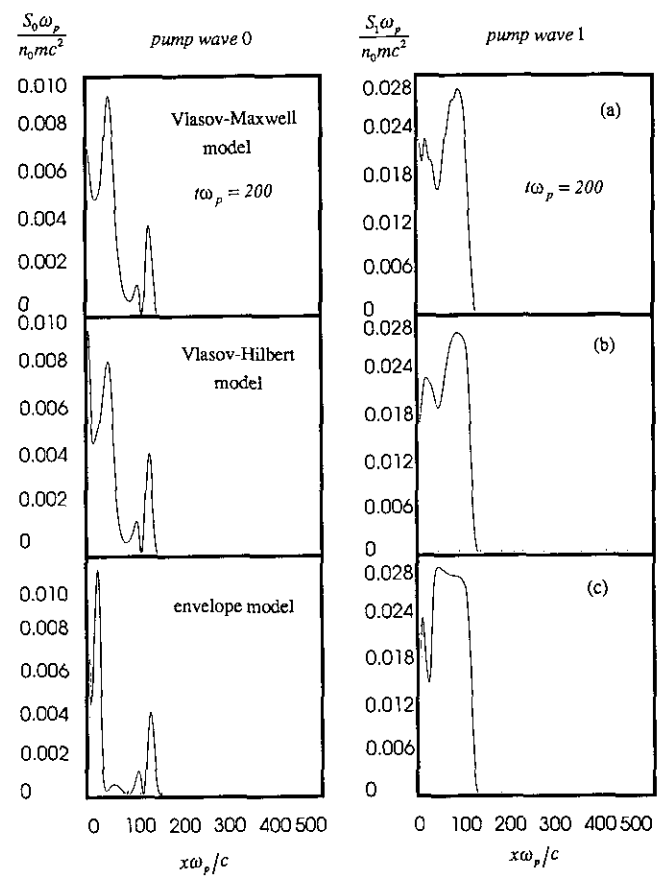

FIG. 3. (a) Envelope of pump waves, computed from the solution of the Vlasov–Maxwell code using a Hilbert transform at time $t\omega_p = 200$. (b) Corresponding results obtained by the Vlasov–Hilbert model in which the Maxwell equations have been replaced by envelope calculation for pump waves. (c) Corresponding results in the case of a three-wave model in which the plasma wave has been described by envelope equation without damping term.

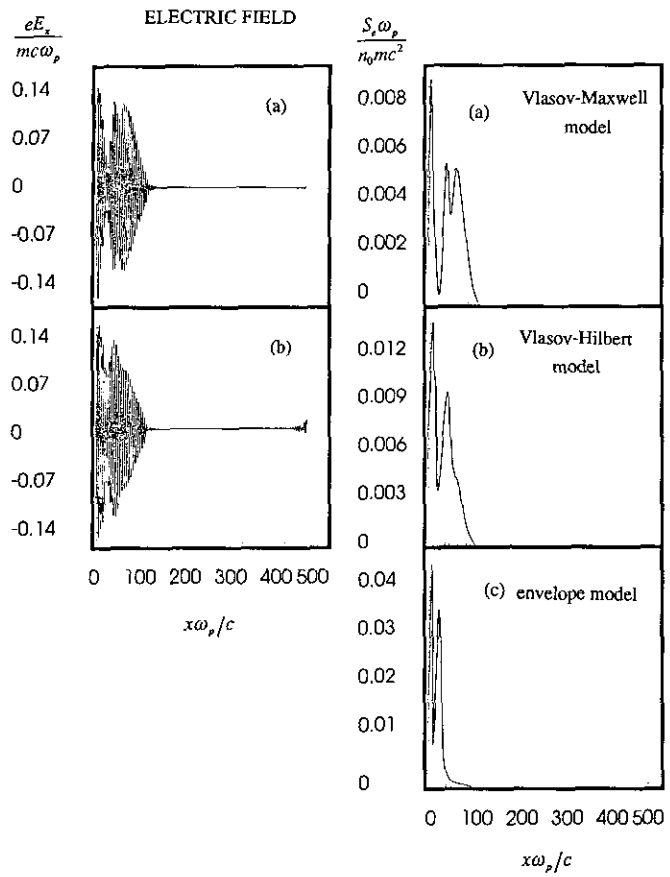

FIG. 4. The longitudinal electric field at time $t\omega_p = 200$ in the case of the Vlasov–Maxwell code, together with its envelope given in action units is plotted in Fig. 3a as a function of space, while the corresponding values given by the Vlasov–Hilbert version are shown in Fig. 3b. The electric field obtained by the three-wave model, without a damping term is shown in Fig. 3c.

amplitude than the Vlasov–Maxwell code, at least for these early times. A significant difference between both Vlasov models and the coupled-wave model result can be seen in the level of the plasma wave. We show in Fig. 4c the plasma wave computed by the fluid model. This difference in mainly caused by the wave–particle interactions that occur in both Vlasov simulations. Figure 5 illustrates that the results obtained by increasing the damping term to a value of $\gamma = 0.0095$ lead to a strong decrease (by a factor 2 in action units) of the amplitude of the electric field, but it must be pointed out that a strong smoothing in electromagnetic mode shapes is occurring in this case, which is not observed in either kinetic simulations. As we have already seen in previous work [5], "ad hoc" damping chosen after the fact, is not a substitute for a real understanding of particle trapping loading of the plasma wave. Even more noticeable is the fact that the spatial advance of the electric field for both Vlasov models is much slower than for the coupled-wave model. It seems likely that the coupled-wave dephasing at the entry is an underestimation, leading to incorrectly rapid pump depletion at the entry and, hence, a reduced ability to stimulate plasma waves further from the entry point.

(B) *Phase Space Representation*

In Ref. [2], we have shown that our Maxwell–Vlasov code is able to give a precise description of the phase space dynamics that is capable of resolving the finest mechanisms of particle acceleration. In Figs. 6a and 6b are shown electron phase space plots at the time $t\omega_p = 200$ for the beatwave-driven plasma wave as modelled by the Vlasov–Maxwell and Vlasov–Hilbert models, respectively. While not identical, the reasonably close correspondence of the two phase space results is highly encouraging.

The separatrices calculated by Eqs. (24) and (25) of Ref. [4] are also drawn. We recall that the separatrix momentum can be easily calculated from the potential obtained from the output of the code. The result given by the Vlasov–Hilbert model is shown in Fig. 6b. The grey shade indicates the magnitude of the particle distribution function $f(x, p_x)$. The solid curves mark the separatrix between the trapped and untrapped particle orbits for the local amplitude of the plasma wave. Although there are some small differences in the behavior of longitudinal electric

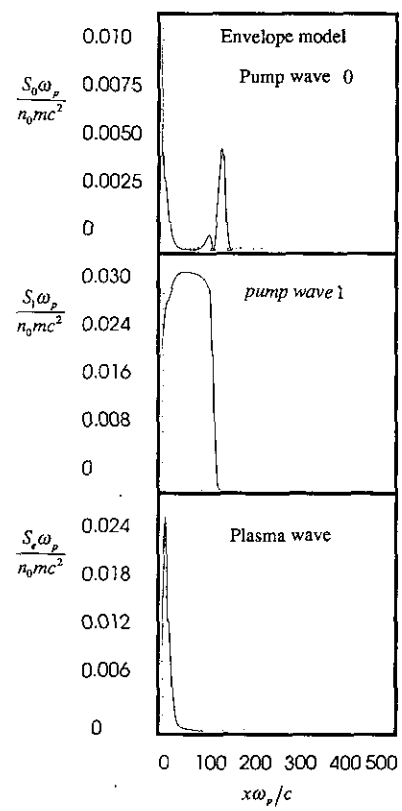

FIG. 5. Both pumps and plasma wave envelopes calculated from the three-wave model, in which the damping term of plasma wave has been chosen to $\gamma = 0.0095$.

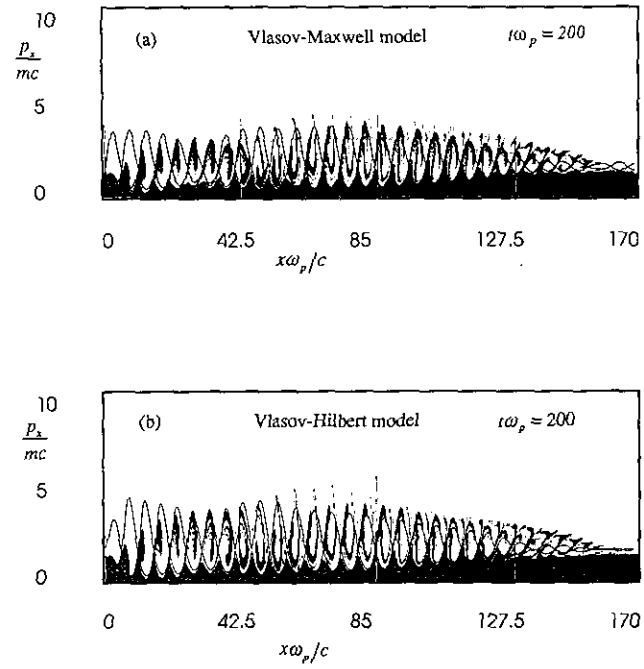

FIG. 6. The phase space representation at time $t\omega_p = 200$ computed by the full electromagnetic Vlasov–Maxwell code is shown in (a), together with the separatrices, which mark the boundary between the trapped and untrapped particle orbits for the local amplitude of plasma wave. The corresponding phase space representation for the Vlasov–Hilbert version, in which we have replaced the Maxwell equations by envelope calculation, is plotted in (b); the particle dynamics seems to account rather well for the complex behavior seen in the full electromagnetic simulation.

fields, the particle dynamics in phase space calculated by using the Vlasov–Hilbert code seems to account rather well for the complex behavior seen in the full electromagnetic simulation. We can see a very striking agreement between the separatrix and the "particle orbits" in both cases. The spirals inside the separatrix implicitly reflect the history of the particles trapped as the plasma wave was built up from zero.

V. AN EXAMPLE OF INTERACTION OF HIGH-FREQUENCY ELECTROMAGNETIC WAVES WITH PLASMA

The final example, given to illustrate the real possibilities of this Vlasov–Hilbert code, is the beat of two very high-frequency electromagnetic waves in plasma, in order to analyze the particle acceleration process comparable to that recently observed in experiment [6]. For economy in this demonstration our pump rise times are chosen to be faster than the experiment. We simulated a beatwave process using pump frequencies of $\omega_0 = 30.01\omega_p$ and $\omega_1 = 28.96\omega_p$. The other numerical parameters are presented in Table II. Here the code is in a regime so extreme that we can only compare it with the mode coupling results due to the fact that the full Vlasov–Maxwell computer burden is prohibitive for electron kinetic effects.

As before, for the numerical experiments presented in Section IV, the plasma was chosen with two electron temperature components, the majority (95%) component with a 15 keV temperature, and a minority component (5%) at 100 keV. (The cold temperature was chosen high enough for electron damping to subdue the usually rapidly growing, but here unwanted, backward Raman instability, while the hot component was enough to ensure sufficient electrons to start the electron trapping and acceleration which is relevant to beatwave acceleration, without any initial beam-plasma instability). Using an action space grid $N_x N_{p_x} = 2048 \times 1024 = 2{,}097{,}152$ points, the CPU time on the Cray-2 computer is 1 μs per time step per grid point, i.e., about 1 h CPU time for a run time up to $500\omega_p^{-1}$. For a plasma length $L = 500\ c/\omega_p$, the grid size is $\Delta x = 0.293\ c/\omega_p$ (the time step is then fixed by the choice of $\Delta x = c\Delta t$, the condition used to start up the instability in the Eulerian Vlasov simulation).

Now we present in Fig. 7 the numerical results obtained from the Vlasov–Hilbert code, at time $t\omega_p = 400$. The figures show the envelope of the pump wave (Fig. 7a) and its corresponding second pump wave (Fig. 7b) in action units, together with the longitudinal electric field (in Fig. 7c) and its corresponding envelope (in Fig. 7d). At that time the penetration of the electromagnetic pump and the nonlinearity is strong enough for the three modes to be present. After the first stage of the instability (the first left-hand structure observed in the electric field is probably due to a too-rapid growth of the pump laser intensity in plasma), the curves exhibit the beginning of the well-known Rosenbluth–Liu oscillatory behavior in which the energy is transferred back and forth between the pump, the idler, and the plasma waves. Comparing these numerical results

TABLE II

Beatwave Experiment Parameters

Pump wave number (0)	$\frac{k_0 c}{\omega_p} = 30$
Pump wave number (1)	$\frac{k_1 c}{\omega_p} = 28.952$
Plasmon wave number	$\frac{k_e c}{\omega_p} = 1.04790$ or $k_e \lambda_D = 0.179$
Pump wave frequency (0)	$\omega_0 = 30.01\omega_p$
Pump wave frequency (1)	$\omega_1 = 28.96\omega_p$
Plasmon wave frequency	$\omega_e = 1.04723\omega_p$
Electron temperature	$T = 15$ keV
Plasmon phase velocity	$\frac{v_\varphi}{c} = \frac{\omega_e}{k_e c} = 0.99933$
Corresponding phase momentum	$\frac{p_\varphi}{mc} = \frac{v_\varphi/c}{\sqrt{1 - v_\varphi^2/c^2}} = 27.36$
Pump quiver "velocity" (0)	$\frac{p_{\mathrm{osc}_0}}{mc} = 0.0999$
Pump quiver "velocity" (1)	$\frac{p_{\mathrm{osc}_1}}{mc} = 0.1035$
Plasma relative density	$\frac{n_e}{n_{\mathrm{crit}}} = 0.0011$

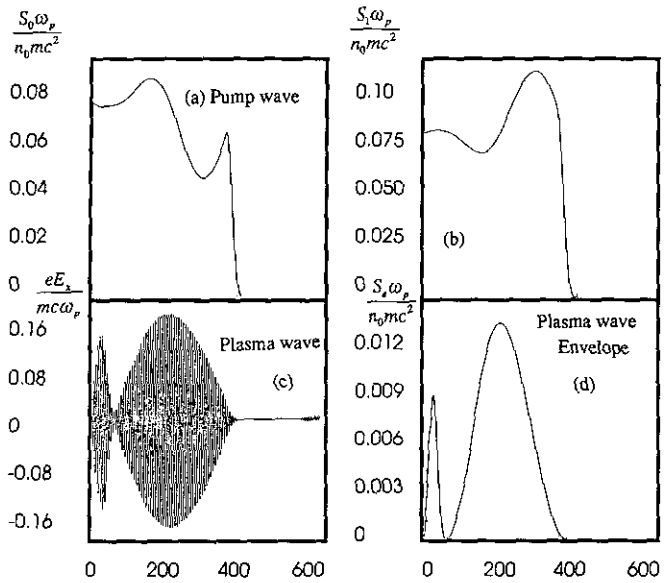

FIG. 7. The envelope of high frequency pump wave is shown in (a), while the lower frequency pump wave envelope is plotted in (b) in action units, at time $t\omega_p = 400$, in the case of high-frequency electromagnetic beatwave obtained from kinetic Vlasov–Hilbert simulations. The corresponding longitudinal electric field is plotted in (c), together with its envelope in action units, showing that the major part of the structure formed is seen to be due to pump depletion/plasma wave building cycles.

with the case of the coupled modes model shown in Fig. 8 (without a damping term) shows similar typical phenomena. It is clear that the general features are well reproduced, except for the amplitude of the electric field action, due to the fact that kinetic effects are not correctly taken into account in the envelope model. The plasma waves are running waves rather than standing waves, so these localized fields are not cavitons, but a more complex result of interaction between the laser pump, the laser idler wave, and the plasma wave. Support of this concept is shown by the fact that similar behavior is seen in coupled mode theory, as shown in Fig. 8.

As remarked at the outset, this method provides a saving of the order $(\omega_{\text{pump}}/\omega_{\text{plasma}})^2$ in computer time, as compared with the direct Vlasov method with the highest space-time resolution required. Due to the Courant condition $\Delta x = c\Delta t$, and the high frequency of the pump wave ($\omega_0 \approx 30\omega_p$), the same simulation results shown in Fig. 7 would require about 900 h CPU time on a Cray-2 computer using a full electromagnetic Vlasov code, to be compared with the results obtained by the Vlasov–Hilbert code.

A limitation of the model in the present case is that cascade processes (i.e., including more sidebands in the envelope equations) are not taken into account here, while recent simulations [9], including relativistic Vlasov–Maxwell and supporting envelope and test particle calculation have shown the possibility that a second Stokes wave may be excited, if the plasma is sufficiently underdense. The energy transfer to the plasma wave is then enhanced by the decay of the Stokes wave. Furthermore, strong depletion of the Stokes wave caused by the down-cascading to the second Stokes component has been observed in Vlasov simulations. An effort to take into account the down-cascading process in the Vlasov–Hilbert model (by adding the necessary cascade modes) is well in hand, and these results should be reported in due course.

VI. SUMMARY AND DISCUSSION

In order to be able to treat the problem of high-frequency electromagnetic waves interacting with a plasma via beatwave-induced plasma waves, we have investigated the replacement of our previous $1\frac{1}{2}$D Vlasov code with full details for both the transverse and longitudinal aspects of the Maxwell equations (which we have now named a Vlasov–Maxwell code) with the much less burdensome option of coupling a longitudinal Vlasov code with the ponderomotive force generated by the beating between the transverse waves (which are treated by usual the slowly varying envelope approximation); this code we have called the Vlasov–Hilbert code.

We have tested this new code in three problems. In the

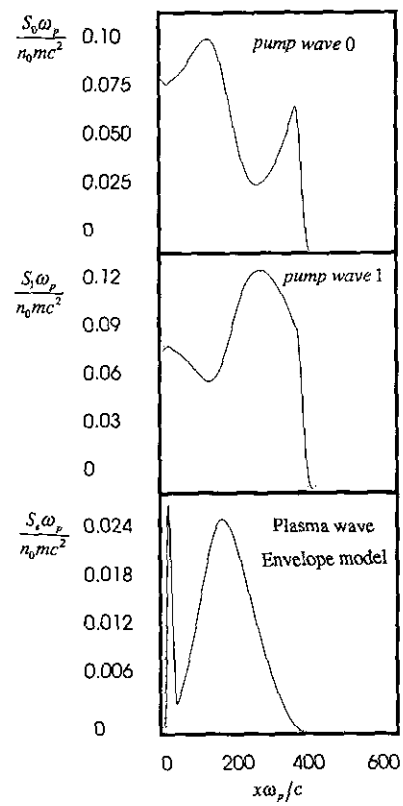

FIG. 8. The corresponding envelopes of pumps and plasma waves obtained by the three-wave model, in which the damping term has been chosen to zero. It is clear that the general features are well reproduced although the amplitude of the electric field is stronger in comparison with the kinetic simulation.

simplest case, that of a spatially periodic initial value case, we find the two Vlasov codes to agree very well and to exhibit the same differences of each with respect to the coupled-oscillator model. In the case of a spatially open system with external drive, while the same statement is generally true, we begin to see some modest but noticeable differences between the two kinds of Vlasov codes which are, however, still much closer to each other than to the coupled wave model. (We suspect, but have yet to demonstrate, that the difference between the two Vlasov codes will be less if the driving wave onsets more slowly.) At high frequency, where the Vlasov–Maxwell code can no longer be used, the differences between the coupled wave and the Vlasov–Hilbert code are of the same character as before, and we expect that the Vlasov–Hilbert code is doing a good job of imitating the Vlasov–Maxwell code at $\frac{1}{900}$ of the cost.

In recent beatwave experiment the electron temperature is lower, close to $T_e \approx 20$ eV. However, envelope equations corresponding to backward Raman scattering can be included in our code without difficulty and numerical results concerning beatwave experiment with beam injection will be presented in a future work. We have also begun to look into cascading (i.e., including more sidebands in the envelope equations) and will be considering stimulated Brillouin scattering [10–11] (probably with ion kinetics and an electron kinetic fluid) and the effects of ion motion in the nonlinearity of coupling between plasma waves [12–13]. However, it should be noted that in the experiments of Ref. [7] the plasma scattering (via the modulational instability) in all directions over a great range of wavenumbers played an essential role, so a realistically useful simulation would have to await an extension to at least two spatial dimensions.

There seems no reason not to try this technique with a particle-in-cell (PIC) code, although the particle noise may pose a problem in producing a reasonable envelope for coupling to the high-frequency transverse modes (spatial filtering may help). The real reward would be if one can generalize a PIC–Hilbert technique to two spatial dimensions, which is liable to be costly for the Vlasov–Hilbert part of the code, because one must calculate a forbiddingly large fraction of phase space with very low electron density.

ACKNOWLEDGMENTS

The authors are indebted to the IDRIS center (Institut du Developpement et des Ressources en Informatique Scientifique, Paris, France) for computer time allocation on the Cray -C98 computer and to the old CCVR center (Palaiseau) for time allocation on the Cray-2 computer. P. Bertrand, A. Ghizzo, and J. Lebas would like to acknowledge the hospitality to the Centre Canadien de Fusion Magnétique of Varennes (Canada). The authors are indebted to Dr. E. Fijalkow, M. R. Feix, S. J. Karttunen, R. R. E. Salomaa, and T. J. H. Pättikangas for interesting discussions on the topic. In addition, T. W. Johnston would like to acknowledge financial support from le Ministère de l'Education du Québec and from the Canadian National and Engineering Research Council.

REFERENCES

1. A. Ghizzo, P. Bertrand, M. Shoucri, T. W. Johnston, E. Fijalkow, and M. R. Feix, *J. Comput. Phys.* **90,** 431 (1990).
2. P. Bertrand, A. Ghizzo, T. W. Johnston, M. Shoucri, E. Fijalkow, and M. R. Feix, *Phys. Fluids B* **2,** 1028 (1990).
3. A. Ghizzo, P. Bertrand, M. Shoucri, T. W. Johnston, E. Fijalkow, and M. R. Feix, *J. Comput. Phys.* **102,** 417 (1992).
4. T. W. Johnston, P. Bertrand, A. Ghizzo, M. Shoucri, E. Fijalkow, and M. R. Feix, *Phys. Fluids B* **4,** 2523 (1992).
5. T. Réveillé, P. Bertrand, A. Ghizzo, J. Lebas, T. W. Johnston, and M. Shoucri, *Phys. Fluids B* **4,** 2665 (1992).
6. K. Clayton, A. Marsh, A. Dyson, M. Everett, A. Lal, W. P. Leemens, R. Williams, and C. Joshi, *Phys. Rev. Lett.* **70,** 37 (1993).
7. F. Amiranoff, M. Laberge, J. R. Marquès, F. Moulin, E. Fabre, B. Cros, G. Matthieussent P. Benkheiri, F. Jacquet, J. Meyer, P. Miné, C. Stenz, and P. Mora, *Phys. Rev. Lett.* **68,** 3713 (1992).
8. B. Cohen, M. Mostrom, D. Nicholson, A. Kaufmann, and B. Langdon, *Phys. Fluids* **18,** 470 (1975).
9. P. Bertrand, A. Ghizzo, S. J. Karttunen, T. J. H. Pättikangas, R. R. E. Salomma, and M. Shoucri, *Phys. Fluids B* **4,** 3590 (1992).
10. G. Bonnaud, *Plasma Phys. Controlled Fusion* **29,** 573 (1987).
11. K. Estabrook, W. L. Kruer, and M. G. Haines, *Phys. Fluids B* **1,** 1282 (1989).
12. H. Pesme, S. J. Karttunen, R. R. E. Salomaa, G. Laval, and N. Silvestre, *Laser Part. Beams* **6,** 199 (1988).
13. J. A. Heikkinen and S. J. Karttunen, *Phys. Fluids* **29,** 1291 (1986).